RSC Mechanochemistry

ROYAL SOCIETY OF CHEMISTRY

PAPER

View Article Online
View Journal

Cite this: DOI: 10.1039/d5mr00163c

Aerobic mechanochemical RAFT copolymerization of thioctic acid with solid monomers

Xiaoyang Shao, Haoyang Feng, Wenjing Liu, Xiaoyu Wang, Chen Wang, Jinhong Han and Zhenhua Wang *

Mechanochemical solid-state radical polymerization still faces significant challenges, primarily due to limited mass transfer and inefficient initiation mechanisms under these conditions. This study proposes a robust mechanochemical approach for preparing biodegradable vinyl copolymers, enabling solvent-free RAFT copolymerization of thioctic acid (TA) with various solid-state monomers—including acrylamide derivatives and styrene derivatives—under aerobic conditions. By utilizing mechanical-to-chemical energy transduction, we achieved programmed dissociation of amine-coordinated alkylborane initiators, thereby enabling precise control over radical generation within a heterogeneous solid matrix. Under optimized ball-milling conditions at 30 Hz, copolymers of *N*-isopropylacrylamide (NiPam) and TA were synthesized with high conversions (up to 81.0%) and narrow dispersities ($Đ$ < 1.61). The system also exhibited broad compatibility with styrenic monomers such as vinylbenzoic acid (VBA), yielding well-defined copolymers. Systematic studies revealed that the coordination strength of the initiator and the structural compatibility of the chain transfer agent (CTA) play critical roles in regulating polymerization kinetics. This work establishes a versatile mechanistic framework for the design of dynamic covalent materials *via* sustainable, solvent-free mechanochemical pathways.

Received 28th December 2025
Accepted 16th March 2026

DOI: 10.1039/d5mr00163c

rsc.li/RSCMechanochem

Introduction

Mechanochemistry has recently transitioned from a primitive grinding technique to a sophisticated synthetic manifold capable of driving complex chemical transformations through direct mechanical force.[1–7] Unlike conventional thermal or photochemical activation, which rely on bulk energy equilibrium, mechanochemical activation facilitates non-equilibrium processes that can circumvent the limitations of monomer solubility,[8,9] thermal sensitivity, and limited light penetration in heterogeneous media.[10–12] The field of polymer science has witnessed extensive research on mechanochemical polymerization in recent years, spanning from traditional mechanochemical radical polymerization to the more recent RDRP (reversible deactivation radical polymerization) approach.[13,14] Ball milling, as a solid-phase reactor, has been extensively studied by researchers. The Pang team reported an ATPR (atom transfer radical polymerization) reaction conducted under ball milling conditions.[15] The intense blending effect generated by ball milling facilitates electron transfer and mass transport, enabling the successful preparation of narrowly dispersed polymethacrylates. The Golder group utilized the redox potential difference generated during ball milling of $BaTiO_3$ to dissociate diarylnium salts, thereby initiating radical polymerization.[16] Subsequent work further optimized and expanded this system to achieve RAFT polymerization, enabling the controlled synthesis of block copolymers from two incompatible monomers.[17] Thus, mechanochemical solid-state polymerization offers unique opportunities to achieve ultra-high effective monomer concentrations and potentially obtain distinctive polymer microstructures.[8,18–23] However, due to the lack of a solvent medium that promotes radical transfer and heat dissipation, it is difficult to maintain control over the polymer molecular weight.[24,25]

Traditional reversible addition-fragmentation chain transfer (RAFT) polymerization, while highly successful in solution,[26–30] faces fundamental bottlenecks when applied to solid matrices *via* conventional initiation methods. Thermal initiation, the most common approach, typically requires elevated temperatures (*e.g.*, using AIBN), which in a solid environment often results in poor heat transfer and localized overheating.[31] This lack of thermal homogeneity leads to broad molecular weight distributions and, critically, can trigger the premature thermal degradation of sensitive monomers such as thioctic acid (TA).[32–36] Thioctic acid possesses a dynamic cyclic disulfide bond with a relatively low ceiling temperature, making it prone to uncontrolled, non-living ring-opening polymerization if exposed to prolonged heating.[37–40] On the other hand, photochemical initiation is plagued by the "shading effect" in opaque or dense solid mixtures.[12] Since light penetration is exponentially attenuated by scattering and absorption within the solid

Frontiers Science Center for Flexible Electronics (FSCFE) & Institute of Flexible Electronics (IFE), Northwestern Polytechnical University, Xi'an, 710072, China

matrix, the effective initiation is restricted to the surface layers, leading to significant kinetic gradients and poor scalability.[41,42]

Mechanochemical activation *via* ball milling offers a transformative solution to these challenges by acting as a non-equilibrium energy manifold.[43–47] By directly converting mechanical shear and impact into chemical potential, it enables the controlled dissociation of initiators without the need for bulk heating,[9,12,20,48] thereby protecting the integrity of thermally sensitive monomers like TA. Furthermore, the high-energy collisions during milling provide rapid interfacial turnover and forced mass transport, effectively mimicking the mixing efficiency of liquid-phase systems within a solid-state environment.[49] This "forced mixing" ensures uniform dispersion of free radicals, overcoming diffusion barriers that cause uncontrolled termination of bulk or solid-state reactions.[9,50]

In this study, aerobic mechanochemical RAFT copolymerization of thioctic acid with solid monomers were demonstrated. By employing amine-coordinated triethylborane (Et_3B) complexes as "latent" initiators, ball milling could trigger the release of triethylborane, subsequently reacts with ambient oxygen—a species usually considered an inhibitor in radical polymerization—to generate a steady flux of initiating radicals.[28,29,50–55] This synergy between mechanical force and oxygen not only eliminates the need for strict deoxygenation but also provides a efficient tool for initiating solid polymerization process by the milling frequency. By integrating these sustainable principles with the precision of RAFT kinetics, this study establishes a robust methodology for the solvent-free synthesis of high-performance functional copolymers, offering a strategic blueprint for the development of the next generation of dynamic covalent and mechanochemically-responsive materials.

Results and discussion

Aerobic mechanochemical RAFT copolymerization

In our previous studies, we reported an aerobic mechanochemical RAFT strategy whose physical mechanism involves the conversion of mechanical energy into radical energy mediated by ambient oxygen. The coordination bond between Et_3B and the amine ligand is broken by mechanical forces from ball milling, releasing ethyl radicals formed from the reaction between Et_3B and oxygen in the vessel, which then initiate the polymerization reaction (Scheme 1).

To clarify the driving force of this initiation, we conducted comprehensive control experiments to differentiate mechanical activation from thermal and photochemical pathways (Table 1). Monitoring the internal temperature of the ball-milling jar revealed an increase of only ~5 °C (from ~25 °C to ~30 °C) after 30 minutes of milling at 30 Hz (Fig. S11). Given that the thermal dissociation temperature of the Et_3B-DMAP complex exceeds 100 °C,[28] the negligible thermal dissipation is insufficient to trigger spontaneous initiation. This was further corroborated by an external heating experiment at 50 °C (Entry 5), which yielded low monomer conversions (TA: 19.5%, NiPam: 9.9%), likely attributed to the intrinsic thermal ring-opening of TA rather than initiator dissociation.

Furthermore, while the complex exhibits photochemical responsiveness under 405 nm irradiation (Entry 6, TA: 36.5%, NiPam: 31.5%), the polymerization efficiency remains significantly lower than that of the mechanochemical standard (Entry 1, Fig. S9, TA: 63.3%, NiPam: 81.0%). These results demonstrate that mechanical force acts as a more efficient energy manifold for solid-state reactions, providing not only the chemical energy for bond scission but also the mechanical energy required for effective radical dispersion and monomer replenishment. The lack of conversion under anaerobic conditions (Entry 4,

Table 1 Aerobic mechanochemical RAFT copolymerization of thioctic acid with solid monomers

Entry[a]	Condition	Conversion[c] (%)
1	Standard	TA: 63.3, NiPam: 81.0
2	Without initiator	TA:13.3, NiPam:11.6
3	Without ball milling	TA:10.6, NiPam:4.7
4	Without oxygen	TA:<5, NiPam:<5
5[b]	Under 50 °C heating	TA:19.5, NiPam:9.9
6[b]	Under 405 nm UV irradiation	TA:36.5, NiPam:31.5

[a] Target degree of polymerization (DP) = 100. $[TA]_0:[NiPam]_0:[ATTC]_0:[Et_3B\text{-}DMAP]_0 = 30:70:1:5$. 25 mL stainless steel jar, 10 mm × 2 stainless steel grinding ball. Ball milling frequency is 30 Hz. Reaction time is 30 min. Ambient conditions served as the experimental conditions. [b] Without ball milling. [c] Conversion was determined by ^1H NMR spectroscopy.

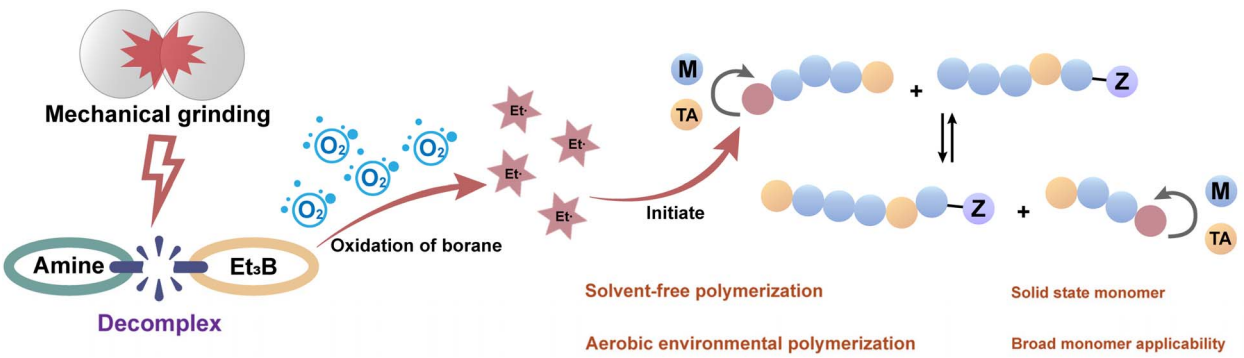

Scheme 1 Reaction mechanism of solid-state mechanochemical copolymerization.

"Without oxygen") confirms that oxygen is not an inhibitor but an indispensable co-initiator. Furthermore, the minimal conversion observed without milling (Entry 3) highlights that the coordination bond is sufficiently stable at ambient conditions, preventing premature radical leakage. This oxygen-tolerant initiation is particularly advantageous for large-scale solid-state synthesis where strict deoxygenation is technically challenging. To further verify that the polymerization proceeds *via* the RAFT mechanism, a control experiment was conducted in the absence of CTA. In this case, uncontrollable molecular weight and broad molecular weight distribution were observed, whereas controlled polymerization behavior was maintained in the presence of CTA (Fig. S12).

Optimization of CTA

The efficiency of RAFT polymerization in the solid state is highly sensitive to the structural compatibility of the chain transfer agent (CTA). Unlike solution polymerization where diffusion is rapid, the CTA in a solid matrix must compete with high local monomer concentrations. We systematically evaluated five CTAs with varying Z and R groups (Table S1, Fig. 1).

Trithiocarbonates, such as ATTC and DDMAT, exhibited superior control compared to dithiobenzoates like CPADB. The success of ATTC is attributed to its balanced electronic properties: the trithiocarbonate Z-group provides moderate stabilization of the intermediate radical, while the carboxyl-containing R-group enhances the interfacial compatibility with polar monomers like NiPam and TA. In contrast, CPADB yielded a bimodal molecular weight distribution (Fig. 1b). We hypothesize that the strongly electron-withdrawing cyanoisopropyl R-group of CPADB leads to a fragmentation rate that is too slow in the high-viscosity solid state, resulting in inefficient re-initiation and the formation of uncontrolled high-molecular-weight fractions. These results underscore that for aerobic mechanochemical RAFT, the CTA must be chosen to match the mechanical flux of radicals to maintain a dynamic equilibrium.

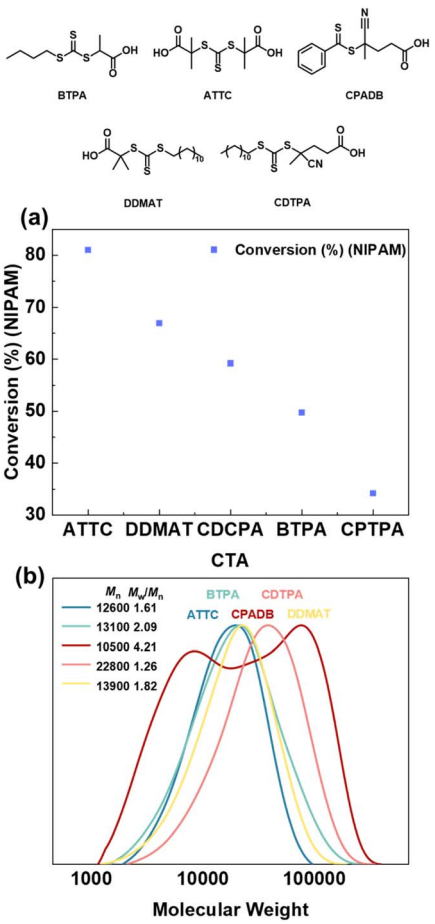

Fig. 1 Solid-state mechanochemical copolymerization with different chain transfer agents. Reaction condition: 25 mL stainless steel jar and 10 mm × 2 stainless steel grinding ball. Ball milling frequency is 30 Hz and reaction time is 30 min. (a) NiPam conversion rates induced by different chain transfer agents. (b) GPC curves of copolymers with different chain transfer agents.

Initiator structure

The stability of the initiator complex plays a crucial role in controlling the aerobic mechanochemical RAFT process. We observed a profound disparity in polymerization control between Et_3B-DMAP and Et_3B-MeOPy, which can be rationalized by their distinct coordination chemistry.

The Et_3B-DMAP complex, benefiting from the strong electron-donating ability of the dimethylamino group ($pK_a \approx 9.2$), exhibits high thermodynamic stability and excellent "mechanochemical latency." In this case, the B–N bond remains intact under ambient storage and quiescent conditions, with radical generation exclusively triggered by the high-energy mechanical impact of 30 Hz milling. In stark contrast, the Et_3B-MeOPy complex, characterized by a weaker coordination bond due to the lower basicity of MeOPy ($pK_a \approx 6.6$), is susceptible to "monomer-induced activation." Specifically, the acidic carboxyl groups of TA can facilitate proton-induced ligand displacement or competitive coordination with the boron center, leading to a spontaneous radical "leak" even in the absence of mechanical force (Table S2). This premature dissociation results in an uncontrolled initial radical concentration, causing rapid chain termination and a significant broadening of the molecular weight distribution ($Đ = 2.72$) (Fig. 2b). These findings suggest that for successful solid-state CRP, the initiator's coordination strength must be meticulously tuned to resist chemical interference from monomeric functional groups, ensuring that the initiation event is strictly gated by mechanical stimuli.

Influence of TA content

The concentration of thioctic acid (TA) in the monomer feed represents a critical variable that modulates both the initiation kinetics and the resulting macromolecular control. Experimental data (Fig. 3) reveal a positive correlation between TA content (ranging from 5% to 30%) and the overall monomer conversion. This trend originates from the chemical synergy between the carboxyl groups of TA and the amine–borane

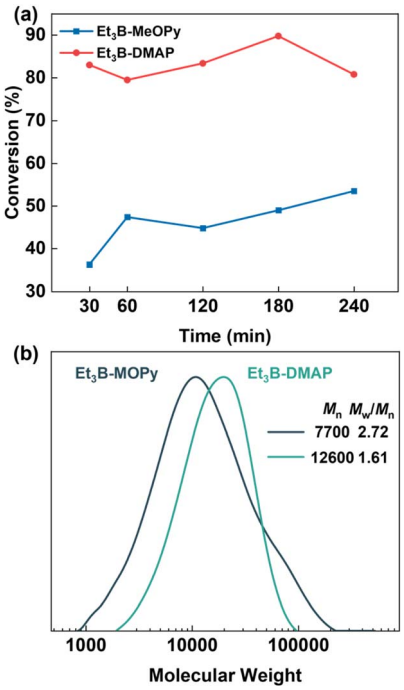

Fig. 2 Effect of latent initiators on mechanochemical copolymerization. Reaction condition: 25 mL stainless steel jar and 10 mm × 2 stainless steel grinding ball. Ball milling frequency is 30 Hz. (a) NiPam conversion rates at different ball milling durations. (b) GPC curves for the 30 min reaction.

complexes. As the TA concentration increases, the elevated proton activity in the heterogeneous mixture promotes the acid-catalyzed dissociation of the B–N coordinative bond, effectively lowering the mechanical energy threshold required for radical generation. Consequently, higher TA loadings lead to a higher steady-state radical concentration and increased conversion rates.

However, this chemically induced acceleration effect has instead impacted the system's polymerization process. A progressive broadening of the dispersity ($Đ$) and an increase in molecular weight (M_n) were observed with increasing TA content (Fig. 3a and b). This deterioration in control is attributed to the increased density of dynamic disulfide bonds within the solid matrix. These disulfide moieties can participate in competitive radical addition and chain transfer events, which interfere with the primary RAFT equilibrium. Furthermore, for the weaker Et_3B-MeOPy initiator, excessive TA content leads to a significant radical burst, resulting in premature termination of the polymer chains and a notable drop in conversion at the highest TA loadings (Fig. 3c). These results underscore that the TA content must be carefully balanced to exploit its self-promoted initiation while maintaining the stringent control required for well-defined copolymers.

Milling frequency

The milling frequency, in conjunction with the mass and size of the milling media, dictates the mechanical energy density and the frequency of collision events, as described by the fundamental mechanochemical parameters established by Peterson and Borchardt. According to these models, the total energy dose is a function of both the collision frequency and the kinetic energy per impact ($E_{imp} \propto m \times v^2$).[13,56] At a relatively low frequency of 10 Hz, the limited energy input results in insufficient interfacial renewal of the solid reactants. This challenge is further exacerbated by the rapid increase in system viscosity as polymerization progresses in this solvent-free environment. Under such conditions, milling media with smaller diameters or lower densities lack the requisite momentum to overcome the cohesive forces of the viscous polymer matrix, leading to stagnant mixing and restricted diffusion of active species. The resulting spatial heterogeneity in radical distribution promotes irreversible termination and compromises the kinetic control of the RAFT process (Table S3). Conversely, at 30 Hz, the use of optimized, higher-density milling media provides

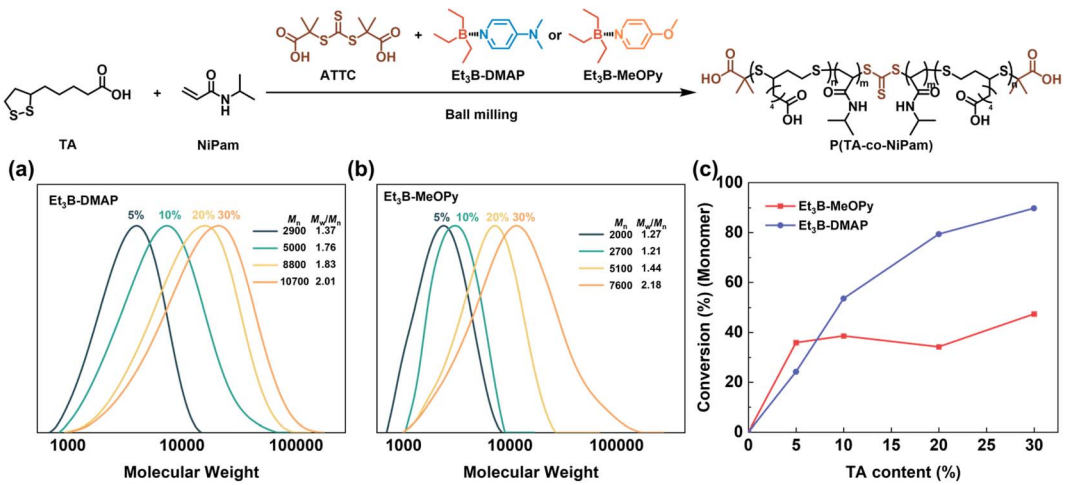

Fig. 3 Effect of TA content. Reaction condition: 25 mL stainless steel jar and 10 mm × 2 stainless steel grinding ball. Ball milling frequency is 30 Hz and reaction time is 1 h. (a) Et_3B-DMAP. (b) Et_3B-MeOPy. (c) Relationship between thioctic acid content and NiPam conversion rate.

a significantly higher mechanical energy dose. These high-intensity collisions generate sufficient shear energy to facilitate continuous particle fragmentation and surface renewal, effectively "plowing" through the viscous matrix to reduce mass transfer resistance. This enhanced mechanical agitation ensures a uniform dispersion of radical species and establishes a consistent radical flux that synchronizes with the rates of monomer propagation and RAFT equilibrium. The observed agreement between $M_{n,\mathrm{GPC}}$ and $M_{n,\mathrm{th}}$ at 30 Hz ($Đ = 1.61$) demonstrates that maintaining a high mechanical energy density—through the synergistic optimization of frequency and milling ball momentum—is essential for ensuring precise molecular weight control in solvent-free, high-viscosity polymerization environments.

Polymerization kinetics

The pseudo-living nature of the aerobic mechanochemical-RAFT process was systematically evaluated through kinetic analysis at 30 Hz (Fig. 4). The linear growth of M_n with total monomer conversion confirms that the concentration of active radical species remains relatively constant throughout the reaction, signifying a well-regulated RAFT equilibrium even under high-intensity mechanical shear.

A closer examination of the kinetic profile reveals a rapid acceleration in polymerization rate during the initial 5 minutes (Fig. 4a). This "initial burst" is attributed to two synergistic factors: first, the high initial partial pressure of oxygen within the milling jar promotes the instantaneous autoxidation of released triethylborane, generating a transiently high radical flux. Second, the fresh surface area created by the initial fragmentation of crystalline monomers facilitates efficient interfacial contact between the initiator, CTA, and monomer particles. As the reaction proceeds, the gradual depletion of oxygen and the increasing viscosity of the reaction matrix lead to a controlled deceleration, transitioning into a steady propagation phase.

Furthermore, a significant disparity in the polymerization kinetics of NiPam and TA was observed. NiPam exhibited a substantially higher propagation rate compared to TA throughout the reaction (Fig. 4a). This divergence is rooted in their fundamental reactivity and growth mechanisms. NiPam undergoes conventional vinyl addition, where the high reactivity of the acrylamide double bond (k_p) and the stability of the carbon-centered secondary radical favor rapid chain growth. In contrast, TA polymerizes *via* a radical ring-opening polymerization (RROP) mechanism of its cyclic disulfide. The kinetics of TA are inherently slower due to the higher steric hindrance surrounding the disulfide bridge and the relatively lower reactivity of the resulting sulfur-centered radicals toward further monomer addition. Moreover, the dynamic disulfide bonds within the TA segments can participate in degenerative chain transfer or backbiting reactions, which effectively acts as an internal kinetic "decelerator." The polymerization kinetics of NiPam during the copolymerization reaction revealed that as the NiPam conversion rate increased, the copolymer molecular weight steadily rose while maintaining a stable molecular weight distribution, demonstrating the controllability of this copolymerization reaction (Fig. 4b and c). In parallel, experiments were conducted with polymerizations targeting higher molecular weights. However, it was observed that the copolymer exhibited a molecular weight around 13 800, accompanied with broad molecular weight distribution (Table S5). Additionally, tailing in the low molecular weight region was observed in the GPC curve, indicating that molecular weight control is limited when the polymerization targets high DP (Fig. S13) due to chain degradation induced by mechanical forces. In subsequent chain extension experiments, a high-molecular-weight peak was observed in the gel permeation chromatography curve following extension(Fig. S14). The chain transfer effect induced by lipoic acid in this system, combined with the presence of chain degradation, likely prevents further extension due to the absence of reactive end groups in the copolymer.

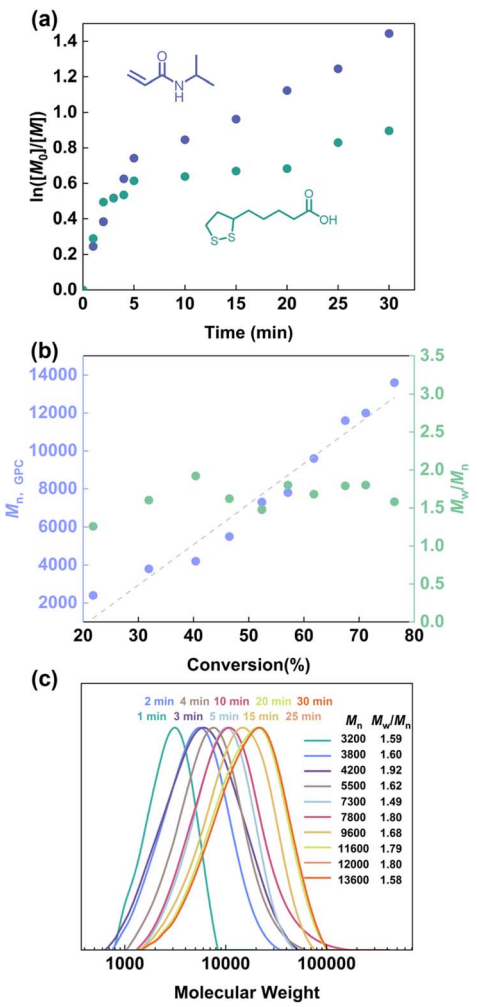

Fig. 4 Kinetics for mechanochemical copolymerization of thioctic acid with NiPam. Reaction condition: 25 mL stainless steel jar and 10 mm × 2 stainless steel grinding ball. Ball milling frequency is 30 Hz. (a) Kinetics of thioctic acid with NiPam with reaction time. (b) Variation of NiPam conversion and $M_{n,\mathrm{GPC}}$. (c) GPC curves from 0–30 min.

Monomer scope

The general applicability of the aerobic mechanochemical RAFT system was systematically validated across eight solid monomers, revealing that the copolymerization efficiency is primarily governed by the molecular compatibility between the monomers and the matching of their radical reactivity (Table S4, Fig. 5). Acrylamide-type monomers, including NiPam, AM, and NPAM, exhibited exceptional reactivity with conversions consistently exceeding 70% (Fig. S15). This high efficiency stems from the excellent molecular miscibility between the polar acrylamide groups and the carboxyl/disulfide moieties of thioctic acid (TA). Under mechanical milling, the propensity for inter-monomer hydrogen bonding facilitates the formation of a homogeneous solid-state "molecular solution," ensuring that the growing radical chain ends have continuous access to both comonomers. Furthermore, the electronic structures of acrylamide radicals match well with the disulfide ring-opening mechanism of TA, leading to favorable crossover reactivity ratios that promote the formation of uniform copolymers.

In contrast, the behavior of styrenic-type monomers was more varied and highly dependent on functional group affinity. Vinylbenzoic acid (VBA) achieved significant conversion and controlled molecular weight ($Đ = 1.39$), which can be attributed to the strong compatibility of its carboxyl group with that of TA. This structural similarity promotes interfacial wetting and co-crystallization-like mixing during milling. However, bulkier or more hydrophobic styrenic derivatives, such as vinylcarbazole (VCz) and sodium styrenesulfonate (SPSS), showed diminished conversions. For these monomers, the lack of polar–polar interactions with the TA-dominated reaction matrix leads to phase segregation at the microscale. This segregation acts as a significant barrier to the RAFT process, as the chain transfer agent and active radicals become trapped within segregated domains, unable to participate in efficient exchange between the diverse monomer species. Consequently, the success of aerobic mechanochemical RAFT copolymerization is not merely a function of mechanical energy input, but a complex interplay of monomer polarity matching and the kinetic synchronization of radical addition across disparate chemical structures.

Conclusion

We have established a robust, aerobic, and solvent-free mechanochemical method for preparing degradable vinyl copolymers, enabling controlled copolymerization of fatty acids with acrylamide and styrene monomers. By leveraging the synergistic interaction between mechanical force and oxygen-mediated alkylborane initiation, we achieved molecular weight control and high monomer conversion rates within a solid matrix. Our findings reveal that the coordination strength of the initiator and the compatibility of CTA structures with the reaction are critical for producing oleic acid copolymers with uniform molecular weight. This work demonstrates that mechanical forces can effectively replace thermal or photochemical triggering mechanisms, opening a more efficient and sustainable pathway for constructing complex dynamic polymers. This method lays the foundation for the green manufacturing of functional materials that are difficult to achieve through conventional solution processes.

Author contributions

Z. W. conceived the idea and designed the experiments. X. S. collaborated with H. F. to conduct polymerization validation experiments, polymerization kinetics studies, monomer scope polymerization experiments, and their corresponding NMR hydrogen spectrum and molecular weight characterization. J. H. participated in the characterization of polymerization experiments using different initiator structures. W. L. provided the synthesis and preparation of various chain transfer agents. X. W. contributed to the preparation of initiators with different structures. C. W. validated control experiments under heating and illumination conditions. X. S. and Z. W. jointly completed the writing of the article. All authors have given approval to the final version of the manuscript.

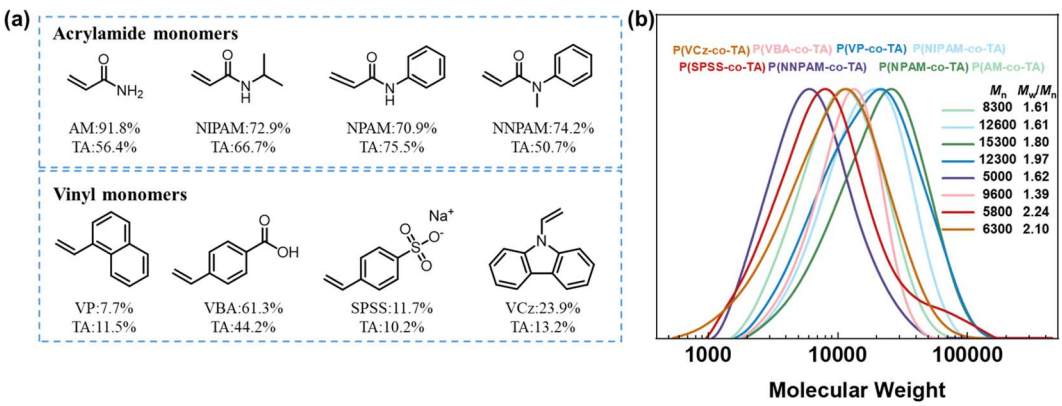

Fig. 5 Mechanochemical copolymerization of solid vinyl monomers and thioctic acid. Reaction condition: 25 mL stainless steel jar and 10 mm × 2 stainless steel grinding ball. Ball milling frequency is 30 Hz and reaction time is 30 min. (a) Monomer conversion rate of acrylamide monomers and vinyl monomers with thioctic acid. (b) The GPC curves of copolymers by copolymerization of different solid monomers with thioctic acid.

Conflicts of interest

There are no conflicts to declare.

Data availability

The date supporting this article have been included as part of the supplementary information (SI). Supplementary information: synthesis steps and NMR hydrogen spectra of chain transfer agents, monomers, and initiators. Temperature changes before and after ball milling in ball mills, conversion rates of different solid monomers, and other polymerization data. See DOI: https://doi.org/10.1039/d5mr00163c.

Acknowledgements

This work was funded by the National Natural Science Foundation of China (5247300) and State Key Laboratory of Advanced Polymer Materials, Sichuan University (sklapm2025-3-13).

Notes and references

1 S. L. James and T. Friščić, *Chem. Soc. Rev.*, 2013, **42**, 7494–7496.
2 J.-L. Do and T. Friščić, *ACS Cent. Sci.*, 2017, **3**, 13–19.
3 Y. Chen, G. Mellot, D. van Luijk, C. Creton and R. P. Sijbesma, *Chem. Soc. Rev.*, 2021, **50**, 4100–4140.
4 J. Batteas, K. G. Blank, E. Colacino, F. Emmerling, T. Friščić, J. Mack, J. Moore, M. E. Rivas and W. Tysoe, *RSC Mechanochem.*, 2025, **2**, 10–19.
5 K. Kubota, Y. Pang, A. Miura and H. Ito, *Science*, 2019, **366**, 1500–1504.
6 H. Xia and Z. Wang, *Science*, 2019, **366**, 1451–1452.
7 E. Colacino, F. Delogu and T. Hanusa, *ACS Sustain. Chem. Eng.*, 2021, **9**, 10662–10663.
8 G. S. Lee, H. S. Lee, N. Kim, H. G. Shin, Y. H. Hwang, S. J. Lee and J. G. Kim, *Macromolecules*, 2024, **57**, 9408–9418.
9 Z. Ren, P. Mei, C. Wang, D. Chen, L. Zhang, W. Zhang, Z. Wang and Z. Zhang, *Macromolecules*, 2025, **58**, 3199–3207.
10 P. Yan, W. Zhao, F. McBride, D. Cai, J. Dale, V. Hanna and T. Hasell, *Nat. Commun.*, 2022, **13**, 4824.
11 V. Martinez, T. Stolar, B. Karadeniz, I. Brekalo and K. Užarević, *Nat. Rev. Chem.*, 2023, **7**, 51–65.
12 C. Wang, W. Fan, Z. Li, J. Xiong, W. Zhang and Z. Wang, *Polym. Chem.*, 2022, **13**, 4908–4914.
13 A. Krusenbaum, S. Grätz, G. T. Tigineh, L. Borchardt and J. G. Kim, *Chem. Soc. Rev.*, 2022, **51**, 2873–2905.
14 A. Rizzo and G. I. Peterson, *Prog. Polym. Sci.*, 2024, **159**, 101900.
15 M. Zhou, Y. Zhang, G. Shi, Y. He, Z. Cui, X. Zhang, P. Fu, M. Liu, X. Qiao and X. Pang, *ACS Macro Lett.*, 2022, **12**, 26–32.
16 S. M. Zeitler, P. Chakma and M. R. Golder, *Chem. Sci.*, 2022, **13**, 4131–4138.
17 P. Chakma, S. M. Zeitler, F. Baum, J. Yu, W. Shindy, L. D. Pozzo and M. R. Golder, *Angew. Chem.*, 2023, **135**, e202215733.
18 G. S. Lee, H. W. Lee, H. S. Lee, T. Do, J.-L. Do, J. Lim, G. I. Peterson, T. Friščić and J. G. Kim, *Chem. Sci.*, 2022, **13**, 11496–11505.
19 J. W. Lee, J. Park, J. Lee, S. Park, J. G. Kim and B. S. Kim, *ChemSusChem*, 2021, **14**, 3801–3805.
20 H. Feng, Z. Chen, L. Li, X. Shao, W. Fan, C. Wang, L. Song, K. Matyjaszewski, X. Pan and Z. Wang, *Nat. Commun.*, 2024, **15**, 6179.
21 H. Y. Cho and C. W. Bielawski, *Angew. Chem.*, 2020, **132**, 14033–14039.
22 Q. Liu, L. Wang and X. He, *Adv. Energy Mater.*, 2023, **13**, 2300798.
23 S. Zou, Y. Yang, J. Wang, X. Zhou, X. Wan, M. Zhu and J. Liu, *Energy Environ. Sci.*, 2024, **17**, 4426–4460.
24 M. D. Nothling, J. E. Daniels, Y. Vo, I. Johan and M. H. Stenzel, *Angew. Chem.*, 2023, **135**, e202218955.
25 S. Han, P. Wen, H. Wang, Y. Zhou, Y. Gu, L. Zhang, Y. Shao-Horn, X. Lin and M. Chen, *Nat. Mater.*, 2023, **22**, 1515–1522.
26 J. Chiefari, Y. Chong, F. Ercole, J. Krstina, J. Jeffery, T. P. Le, R. T. Mayadunne, G. F. Meijs, C. L. Moad and G. Moad, *Macromolecules*, 1998, **31**, 5559.
27 G. K. Clothier, T. R. Guimarães, S. W. Thompson, J. Y. Rho, S. Perrier, G. Moad and P. B. Zetterlund, *Chem. Soc. Rev.*, 2023, **52**, 3438–3469.
28 Z. Chen, Y. Du, X. Li and X. Pan, *Macromolecules*, 2024, **57**, 4192–4198.
29 C. Lv, C. He and X. Pan, *Angew. Chem.*, 2018, **130**, 9574–9577.
30 R. Zhao, C. Wang, K. Huang, L. Li, W. Fan, Q. Zhu, H. Ma, X. Wang, Z. Wang and W. Huang, *J. Am. Chem. Soc.*, 2023, **145**, 26532–26539.
31 S. Vouyiouka, E. Karakatsani and C. Papaspyrides, *Prog. Polym. Sci.*, 2005, **30**, 10–37.
32 K. R. Albanese, P. T. Morris, J. Read de Alaniz, C. M. Bates and C. J. Hawker, *J. Am. Chem. Soc.*, 2023, **145**, 22728–22734.
33 Y. Okayama, P. Morris, K. Albanese, S. Olsen, A. Mori, J. R. de Alaniz, C. M. Bates and C. J. Hawker, *J. Polym. Sci.*, 2025, **63**, 1345–1351.
34 P. T. Morris, K. Watanabe, K. R. Albanese, G. T. Kent, R. Gupta, M. Gerst, J. Read de Alaniz, C. J. Hawker and C. M. Bates, *J. Am. Chem. Soc.*, 2024, **146**, 30662–30667.
35 K. R. Albanese, J. R. de Alaniz, C. J. Hawker and C. M. Bates, *Polymer*, 2024, **304**, 127167.
36 K. R. Albanese, Y. Okayama, P. T. Morris, M. Gerst, R. Gupta, J. C. Speros, C. J. Hawker, C. Choi, J. R. de Alaniz and C. M. Bates, *ACS Macro Lett.*, 2023, **12**, 787–793.
37 Q. Zhang, C.-Y. Shi, D.-H. Qu, Y.-T. Long, B. L. Feringa and H. Tian, *Sci. Adv.*, 2018, **4**, eaat8192.
38 Q. Zhang, Y.-X. Deng, H.-X. Luo, C.-Y. Shi, G. M. Geise, B. L. Feringa, H. Tian and D.-H. Qu, *J. Am. Chem. Soc.*, 2019, **141**, 12804–12814.
39 Y. Deng, Q. Zhang, C. Shi, R. Toyoda, D.-H. Qu, H. Tian and B. L. Feringa, *Sci. Adv.*, 2022, **8**, eabk3286.
40 Q. Zhang, D.-H. Qu, B. L. Feringa and H. Tian, *J. Am. Chem. Soc.*, 2022, **144**, 2022–2033.
41 J. R. S. Brownson, in *Solar Energy Conversion Systems*, ed. J. R. S. Brownson, Academic Press, Boston, 2014, pp. 41–66, DOI: 10.1016/B978-0-12-397021-3.00003-X.

42 K. S. Schmitz, in *Physical Chemistry*, ed. K. S. Schmitz, Elsevier, Boston, 2018, pp. 183–367, DOI: 10.1016/B978-0-12-800513-2.00001-2.
43 X. Xin, J. Geng, D. Zhang, H. T. Ang, H. Wang, Y. Cheng, Y. Liu, R. W. Toh, J. Wu and H. Wang, *Nat. Synth.*, 2025, **4**, 177–187.
44 I. R. Speight, K. J. Ardila-Fierro, J. G. Hernández, F. Emmerling, A. A. Michalchuk, F. García, E. Colacino and J. Mack, *Nat. Rev. Methods Primers*, 2025, **5**, 29.
45 O. F. Jafter, S. Lee, J. Park, C. Cabanetos and D. Lungerich, *Angew. Chem., Int. Ed.*, 2024, **63**, e202409731.
46 G. I. Peterson, *Angew. Chem.*, 2025, **137**, e202512324.
47 A. A. Michalchuk and T. Friščić, *RSC Mechanochem.*, 2025, **2**, 333–335.
48 Z. Ren, C. Ding, R. Ding, J. Wang, Z. Li, R. Tan, X. Wang, Z. Wang and Z. Zhang, *ACS Macro Lett.*, 2023, **12**, 1159–1165.
49 M. F. Rappen, J. Maeder, S. Graetz and L. Borchardt, *RSC Mechanochem.*, 2026, **3**, 235–242.
50 H. Feng, X. Shao and Z. Wang, *ChemPlusChem*, 2024, **89**, e202400287.
51 Y. Wang, Q. Wang and X. Pan, *Cell Rep. Phys. Sci.*, 2020, **1**, 100073.
52 C. Ollivier and P. Renaud, *Chem. Rev.*, 2001, **101**, 3415–3434.
53 C. Lv, Y. Du and X. Pan, *J. Polym. Sci.*, 2020, **58**, 14–19.
54 V. Darmency and P. Renaud, in *Radicals in Synthesis I*, Springer, 2006, pp. 71–106.
55 C.-N. Lv, N. Li, Y.-X. Du, J.-H. Li and X.-C. Pan, *Chin. J. Polym. Sci.*, 2020, **38**, 1178–1184.
56 S. Cha and G. I. Peterson, *Macromolecules*, 2025, **58**, 9944–9951.